JOURNAL OF MATERIALS SCIENCE 24 (1989) 3976–3983

Powder neutron diffraction study of the thermal expansion of a K-substituted cordierite

D. MERCURIO, P. THOMAS, J. P. MERCURIO, B. FRIT
Laboratoire de Chimie Minérale Structurale (U.A-C.N.R.S. no. 320), Faculté des Sciences, 123 Avenue A. Thomas, 87060 Limoges Cedex, France

Y. H. KIM
Division of Material Science and Engineering, Korea Advanced Institute of Science and Technology, P.O. Box 131, Cheongryang-Ri, Seoul, Korea

G. ROULT
D.R.F.G.-SPH/S, C.E.N. Grenoble, 85 X, 38041 Grenoble Cedex, France

A structural study of a potassium-substituted cordierite with $K_{0.5}Mg_2Al_{4.5}Si_{4.5}O_{18}$ formula was performed between 20 and 825° C using a time-of-flight powder neutron diffraction technique, on sintered samples obtained by glass crystallization. The thermal evolution of this compound is essentially of the same nature as for pure hexagonal cordierite, but is very dependent on the presence of potassium atoms within the channels. The very low value of the thermal expansion coefficient ($\bar{\alpha} = 0.4 \times 10^{-6}\,K^{-1}$ between 20 and 825° C) results from an opposite evolution of the *a* and *c* lattice parameters which may be explained in terms of a reorganization and a regularization of (Al, Si)O_4 and MgO_6 polyhedra. It strongly depends on the Al/Si ordering degree.

1. Introduction

Ceramics based on cordierite, $Mg_2Al_4Si_5O_{18}$ already have numerous applications as electrical insulators and low-expansion refractories, due to their high resistivity ($\simeq 10^{12}\,\Omega m$) and to their very low linear thermal expansion coefficient ($\simeq 1$ to $2 \times 10^{-6}\,K^{-1}$ between room temperature and 1000° C). As they also exhibit dielectric constants in the range 4 to 6 and low dielectric losses ($\simeq 10^{-4}$) they are promising materials as substrates for electronic devices, especially as packaging materials [1–3]. Magnesium cordierite occurs in two polymorphic forms: the high-temperature disordered hexagonal form (space group P6/mmc), isostructural with beryl, stable between 1450° C and its melting point ($\simeq$ 1460° C), and the low-temperature ordered orthorhombic form (space group Cmcc) stable below 1450° C [4, 5]. Numerous studies have been carried out in order to elucidate the mechanism of the thermal expansion of both polymorphs, in natural and synthetic cordierites, either pure or substituted [6–17]. Nevertheless, little attention has been devoted so far to alkali-substituted cordierites [14–17].

The work presented in this paper is a part of a general study of the influence of alkali substitution on the relative stabilities of the two polymorphs and on the thermal expansion of the hexagonal form, which is systematically lower than the orthorhombic one [12–14]. It is concerned with a neutron diffraction structural analysis, as a function of temperature, of hexagonal potassium-substituted cordierite with composition: $K_{0.5}Mg_2Al_{4.5}Si_{4.5}O_{18}$ (labelled MK25 in the text).

2. Experimental procedure

Weighed quantities of reagent-grade SiO_2xH_2O, Al_2O_3, MgO and K_2CO_3, corresponding to the nominal composition $K_{0.5}Mg_2Al_{4.5}Si_{4.5}O_{18}$, were ball-milled for 2 h in a plastic bottle. Large bars, obtained by cold pressing at 50 MPa, were sintered at 1300° C for 2 h, melted in an oxhydric flame, and quenched into cold water. The glass pieces so formed were ball-milled for 2 h and uniaxially pressed into large bars ($9 \times 9 \times 65\,mm^3$) necessary for neutron diffraction experiments. These pressed samples were then heated again for 2 h at 1000° C and 2 h at 1160° C. Such a procedure, while ensuring a complete crystallization (checked by differential thermal and X-ray diffraction analyses) gave pure hexagonal cordierite. X-ray fluorescence analysis of the crystallized samples did not show any significant deviation from the nominal composition.

The structural study was performed at the C.E.N., Grenoble, between 20 and 825° C, using a time-of-flight powder neutron diffraction technique. This method, described elsewhere in detail [18], presents several advantages, mainly

1. the whole spectrum is recorded as a function of time at a fixed scattering angle ($2\theta = 90°$);
2. the resolution is excellent over a larger range of interreticular spacings than for conventional diffraction techniques;
3. a large number of reflections are obtained (82 for the present study) with a constant and very good resolution ($\simeq 3 \times 10^{-5}$ nm).

The powder diffraction patterns, recorded at 20,

0022–2461/89 $03.00 + .12

275, 550 and 825° C, were fitted to calculated ones, using a full profile analysis programme (Rietveld method modified for time-of-flight neutron diffraction data) [19], in order to minimize the profile discrepancy factor

$$R_p = \sum_i \frac{|y_i - y(\lambda_i)|}{\sum_i y_i}$$

where y_i is the observed value at the i channel, and $y(\lambda_i)$ is the calculated value of the fitting function at the same i channel. The calculations were carried out in the P6/mmc group, using the structural data of Kim *et al.* [14] as starting values and the following coherent scattering lengths: 0.367, 0.5375, 0.4149, 0.3449 and 0.5805 (10^{-5} nm) for potassium, magnesium, silicon, aluminium and oxygen, respectively. In each case, 16 variables were refined simultaneously, including: lattice parameters, scale factor, atomic coordinates not fixed by the space group, isotropic thermal coefficients, occupancies (Si/Si–Al) of the tetrahedral sites T(1) and T(2), constrained to respect the chemical composition. According to the results of the X-ray fluorescence analysis, the occupancy factor of the potassium site was fixed to 1/4. The refinements all converged to R_p values less than 5% (Table I).

3. Results and discussion

3.1. Structure at room temperature

The neutron diffraction pattern at room temperature, illustrating the fit obtained is shown in Fig. 1. The refined structural parameters are listed in Table I and the main interatomic distances and bond angles are reported in Table II.

A projection along the c-axis of the structure at room temperature is shown in Fig. 2. The polyhedra arrangement ($T(1)O_4$ and $T(2)O_4$ tetrahedra and MgO_6 octahedra) is shown in Fig. 3. It is typical of the hexagonal pure cordierite framework. It consists of six-membered rings of $T(2)O_4$ tetrahedra, centred at the origin, lying in the $x0y$ plane and stacked one above the other (successive rings are rotated $\simeq$ 30° relative to each other about the c-axis). Rings are linked to each other, laterally and vertically by $T(1)O_4$ tetrahedra and MgO_6 octahedra. These linking polyhedra, by sharing edges, form a bidimensional network of large overlapping 12-membered rings ($6T(1)O_4$–6 MgO_6) parallel to $x0y$. The alternate sequence along the c-axis of $T(2)O_4$ (at $z = 0, \frac{1}{2}$) and $T(1)O_4$–MgO_6 (at $z = \frac{1}{4}, \frac{3}{4}$) sheets with respective heights $H_{T(2)}$ and H_M is shown in Fig. 3b.

The ring stacking produces large channels, parallel to the c-axis, in which potassium atoms, statistically

TABLE I Final structural parameters for MK25 cordierite (standard deviations are given in parentheses)

Sites		20° C	275° C	550° C	825° C
Mg	x	1/3	1/3	1/3	1/3
(4c)	y	2/3	2/3	2/3	2/3
	z	1/4	1/4	1/4	1/4
	B (10^{-2} nm^2)	1.28(17)	1.40(18)	1.63(19)	3.42(19)
T(1)	x	1/2	1/2	1/2	1/2
(6f)	y	1/2	1/2	1/2	1/2
	z	1/4	1/4	1/4	1/4
	B (10^{-2} nm^2)	0.85(14)	0.08(14)	0.34(14)	0.58(14)
T(2)	x	0.374 8(8)	0.374 1(8)	0.373 8(8)	0.375 3(5)
(12i)	y	0.263 9(8)	0.267 8(7)	0.266 8(7)	0.270 1(5)
	z	0	0	0	0
	τ(Si)	0.47(3)	0.48(3)	0.51(3)	0.68(3)
	B (10^{-2} nm^2)	0.57(9)	0.04(9)	1.19(10)	0.42(8)
O(1)	x	0.486 5(3)	0.485 0(3)	0.485 1(4)	0.483 8(3)
(24m)	y	0.349 2(3)	0.348 9(3)	0.348 7(4)	0.347 9(3)
	z	0.143 9(3)	0.145 2(3)	0.145 4(4)	0.145 7(3)
	B (10^{-2} nm^2)	1.37(7)	1.21(7)	1.59(7)	1.93(7)
O(2)	x	0.228 7(4)	0.228 5(4)	0.228 9(4)	0.229 3(4)
(12i)	y	0.302 0(4)	0.303 6(4)	0.304 3(4)	0.305 2(4)
	z	0	0	0	0
	B (10^{-2} nm^2)	1.65(9)	1.83(9)	2.15(9)	2.89(9)
K	x	0	0	0	0
(4e)	y	0	0	0	0
	z	0.188 5(31)	0.195 3(27)	0.199 8(48)	0.202 3(48)
	B (10^{-2} nm^2)	2.90(103)	1.75(94)	2.72(101)	7.99(159)
a(nm)		0.979 10(3)	0.979 49(3)	0.979 74(3)	0.980 26(3)
c(nm)		0.939 69(4)	0.938 86(4)	0.938 84(4)	0.938 34(4)
v(nm^3)		0.780 13	0.780 07	0.780 45	0.780 86

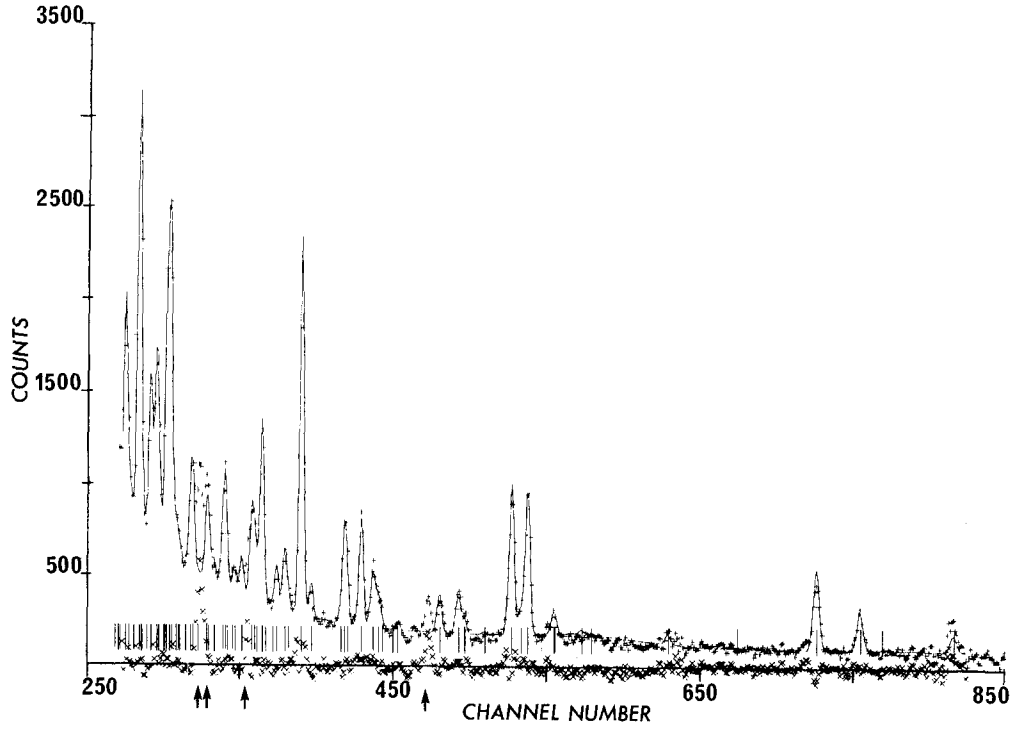

Figure 1 Neutron diffraction patterns for $K_{0.5}Mg_2Al_{4.5}Si_{4.5}O_{18}$ hexagonal cordierite (+) observed at 20° C, (−) calculated and ($I_o - I_c$: x) the difference. The vertical marks show the calculated positions of the reflections, and the arrows the strongest reflections of mullite impurities which were not taken into account for the refinement.

distributed among the 4e positions ($\tau = 0.25$) are located. Each potassium atom is tightly bound to six nearest O(2) atoms of the same closest ring (K–O(2) $\simeq$ 0.32 nm) and more loosely bound to six O(2) atoms of the next ring (K–$O(2)^3$ $\simeq$ 0.40 nm). The K–O(1) distances are longer than the K–O(2) ones: $\simeq$0.43 and $\simeq$0.45 nm for the closest ring and the next one, respectively (see Table II).

As noticed by Predecki *et al.* [9, 13] for pure cordierite, ideal $T(1)O_4$–MgO_6 rings (i.e. built up with regular tetrahedra and octahedra) would not be large enough to fit around the six-membered $T(2)O_4$ rings. They are therefore severely distorted: the T(1)–O_4 tetrahedra are elongated along one of their $\bar{4}$ axis parallel to the $x0y$ plane (their projection along the c-axis is rectangular and not square) and the MgO_6 octahedra are stretched isotropically along the same basal plane (however, the $T(1)O_4$ tetrahedra keep a height in the c direction $H_{T(1)} = H_M = 0.1994$ nm and an $O(1)$–$O(1)^2$ edge length = 0.2830 nm of quite the same order as for a regular tetrahedron with the same cation–anion distance (0.1995 and 0.2835 nm, respectively) whereas the MgO_6 octahedra are considerably flattened along this direction with a height $H_M = 0.1994$ nm strongly shorter than expected for a regular octahedron (i.e. 0.2423 nm).

The distortion of these two polyhedra is evidenced by the departures from ideal values of O–T(1)–O and O–Mg–O bond angles and by the bond-angle distortion indices, σ, reported, respectively, in Tables II and III. σ values were calculated from the following expression [20, 21]

$$\sigma^2 = \sum_{i=1}^{m} (\theta_i - \theta_0)^2/(m - 1)$$

where θ_0 is the undistorted bond angle subtended by

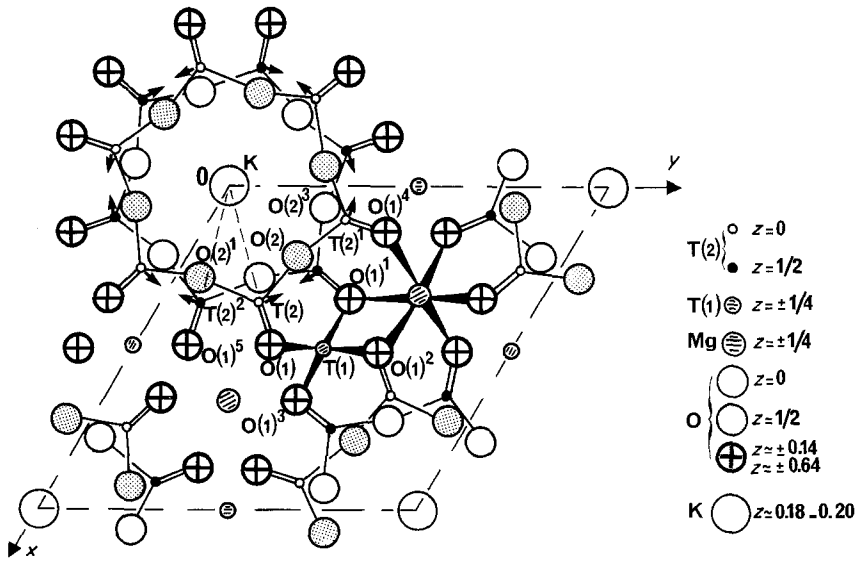

Figure 2 Projection along the c-axis of the MK 25-substituted cordierite structure.

TABLE II Main interatomic distances (nm) and bond angles (deg) for MK25 cordierite (standard deviation in parentheses)

Distances or bond angles	20° C	275° C	550° C	825° C
$T(2)-T(2)^1$	0.326(1)	0.327(1)	0.327(1)	0.329(1)
$T(2)-T(2)^2$	0.493(1)	0.495(1)	0.495(1)	0.496(1)
T(2)–T(1)	0.3087(5)	0.3065(5)	0.3071(5)	0.3053(4)
T(2)–Mg	0.3494(5)	0.3506(5)	0.3507(5)	0.3504(4)
T(1)–Mg	0.2827	0.2828	0.2828	0.2830
T(2)–K	0.371(1)	0.375(1)	0.377(1)	0.379(2)
T(1)–K	0.4929(1)	0.4924(1)	0.4921(1)	0.4922(1)
K–O(2) } (× 6)	0.320(1)	0.325(1)	0.328(1)	0.330(2)
$K-O(2)^3$ }	0.396(1)	0.392(1)	0.390(1)	0.388(2)
⟨K–O⟩	0.358	0.358	0.359	0.359
K–O(1) } (× 6)	0.427(1)	0.427(1)	0.427(1)	0.427(1)
K–O(1) }	0.453(1)	0.450(1)	0.449(1)	0.447(2)
T(1)–O(1) (× 4)	0.1731(4)	0.1721(4)	0.1722(4)	0.1723(3)
$O(1)-O(1)^1$ (× 2)	0.3065(8)	0.3034(8)	0.3034(6)	0.3026(7)
$O(1)-O(1)^3$ (× 2)	0.2562(8)	0.2553(8)	0.2551(6)	0.2559(7)
$O(1)-O(1)^2$ (× 2)	0.2830(8)	0.2824(8)	0.2830(6)	0.2836(7)
⟨O–O⟩ (T(1))	0.2819	0.2804	0.2805	0.2807
T(2)–O(1) (× 2)	0.1676(7)	0.1675(6)	0.1679(6)	0.1664(5)
T(2)–O(2)	0.1649(7)	0.1630(7)	0.1634(6)	0.1630(6)
$T(2)-O(2)^1$	0.1631(7)	0.1654(7)	0.1644(6)	0.1670(6)
⟨T(2)–O⟩	0.1658	0.1658	0.1659	0.1657
$O(2)-O(2)^1$	0.2671(9)	0.2682(9)	0.2689(4)	0.2697(7)
O(1)–O(2) (× 2)	0.2692(6)	0.2693(6)	0.2694(4)	0.2687(5)
$O(1)-O(2)^1$ (× 2)	0.2742(6)	0.2728(6)	0.2725(4)	0.2716(5)
O(1)–O(1)	0.2704(8)	0.2726(8)	0.2730(6)	0.2734(7)
⟨O–O⟩ (T(2))	0.2707	0.2708	0.2709	0.2706
Mg–O(1) (× 6)	0.2098(4)	0.2104(4)	0.2103(3)	0.2109(3)
$O(1)^1-O(1)^4$ (× 3)	0.2877(8)	0.2866(8)	0.2861(6)	0.2855(7)
$O(1)^1-O(1)^2$ (× 3)	0.2562(8)	0.2553(8)	0.2551(6)	0.2559(7)
$O(1)^2-O(1)^4$ (× 6)	0.3198(8)	0.3222(8)	0.3219(6)	0.3235(7)
⟨O–O⟩ (Mg)	0.2959	0.2966	0.2963	0.2971
$O(1)^1-T(1)-O(1)^2$ (× 2)	95.47	95.75	95.57	95.94
$O(1)^1-T(1)-O(1)^3$ (× 2)	109.66	110.27	110.48	110.78
$O(1)^1-T(1)-O(1)$ (× 2)	124.62	123.59	123.58	122.80
⟨O–T(1)–O⟩	109.92	109.87	109.88	109.84
$O(2)^1-T(2)-O(2)$	109.06	109.54	110.21	109.65
$O(2)^1-T(2)-O(1)$ (× 2)	111.91	110.05	110.16	109.07
O(2)–T(2)–O(1) (× 2)	108.12	109.12	108.78	109.30
O(1)–T(2)–O(1)	107.58	108.92	108.72	110.43
⟨O–T(2)–O⟩	109.45	109.47	109.47	109.47
$O(1)-Mg-O(1)^3$ (× 3)	75.22	74.67	74.70	74.72
$O(1)-Mg-O(1)^5$ (× 3)	86.56	85.84	85.74	85.18
$O(1)^3-Mg-O(1)^5$ (× 6)	99.28	99.90	99.93	100.18
⟨O–Mg–O⟩	90.09	90.08	90.08	90.07
$T(2)-O(2)-T(2)^1$	169.06	169.57	170.21	169.65
T(2)–O(1)–T(1)	129.96	128.98	129.04	128.63
$T(2)-O-T(2)^{2*}$	26.52	27.79	27.73	28.47

*The value given is not the real value of the $T(2)-O-T(2)^2$ angle but the value of its projection on to the $x0y$ plane.

an edge of the polyhedron at the centre atom (e.g. 109.47° for a tetrahedron and 90° for an octahedron), θ_i is the corresponding angle observed for the distorted polyhedron, and m is the total number of edges (e.g. 6 for a tetrahedron, 12 for an octahedron). When there is no distortion, $\sigma = 0$.

The mean cation–anion and anion–anion distances in each kind of polyhedron, for the MK25 cordierite and for a pure hexagonal cordierite prepared under the same conditions and studied with nearly the same neutron diffraction technique [9], are reported in Table IV. We can see that the insertion of potassium atoms within the channels results logically, in an increase of the unit-cell parameters, in an expansion of the $T(1)O_4$ and $T(2)O_4$ tetrahedra, richer in aluminium

TABLE III Distortion indices, σ, at various temperatures, for bond angles in $T(1)O_4$, $T(2)O_4$ and MgO_6 polyhedra, in (a) our MK25 cordierite and (b) pure cordierite [9]

(a) MK25

	$\sigma_{20°C}$	$\sigma_{275°C}$	$\sigma_{550°C}$	$\sigma_{825°C}$
T(1)	13.05	12.46	12.54	12.04
T(2)	1.96	0.50	0.78	0.52
Mg	10.48	11.05	11.07	11.25

(b) Pure cordierite [9]

	$\sigma_{22°C}$	$\sigma_{228°C}$	$\sigma_{500°C}$	$\sigma_{750°C}$
T(1)	12.33	11.17	11.98	11.71
T(2)	1.75	1.69	1.87	2.04
Mg	10.79	10.92	10.99	11.23

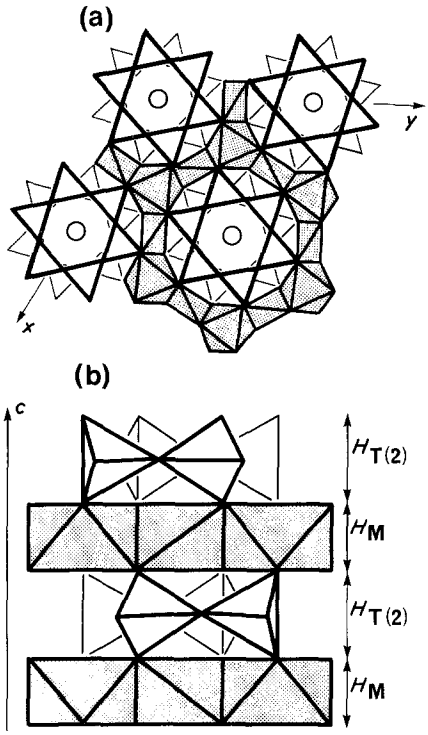

Figure 3 Schematic representation of the hexagonal cordierite structure viewed (a) along the *c*-axis, (b) normal to the *c*-axis.

atoms, and in a small contraction of the MgO_6 octahedron.

3.2. Thermal expansion

The lattice thermal expansion of the substituted MK25 cordierite is compared to those of some pure hexagonal cordierites in Fig. 4. The main feature that can be pointed out in comparison with the other hexagonal cordierites, is the smaller increase of $\Delta a/a$ without significant difference in the behaviour of $\Delta c/c$.

TABLE IV Comparison of mean cation–anion and anion–anion distances in the three polyhedra of MK 25 and pure hexagonal cordierites (nm unit)

	Pure hexagonal cordierite [9]	MK 25 (This work)
a	0.977 28	0.979 10(3)
c	0.934 89	0.939 69(4)
⟨T(2)–O⟩	0.164 8	0.165 8
⟨O–O⟩ (T(2) site)	0.268 5	0.270 7
⟨T(1)–O⟩	0.172 1	0.173 1(4)
⟨O–O⟩ T(1) site)	0.280 4	0.281 9
⟨Mg–O⟩	0.210 6	0.209 8(4)
⟨O–O⟩ (Mg site)	0.297 0	0.295 9

This leads to a smaller evolution of the unit-cell volume and therefore of the linear thermal expansion coefficient, as shown in Fig. 5. A slight contraction, associated with an abnormally low thermal agitation of the T(1) and T(2) cations (see Table I), is even observed at 275° C, indicating that the polyhedral network is particularly stable at this temperature.

If we except the O(1) and K atoms, which move preferentially along the *c* direction, the other atoms move essentially in the basal $x0y$ plane. In order to visualize the structural changes with increasing temperature, the displacements of the atoms in the $x0y$ plane from 20 up to 825° C, are shown magnified 20 times in Fig. 6a. This representation, very useful for the comparison of the relative movements of atoms, is not of course representative of their actual positions.

As clearly indicated by the increase of the projection of the T(2)–O–T(2)[2] angle (Table II and Fig. 2), the T(2) atoms of successive six-membered rings ($z = 0$ and $z = \frac{1}{2}$) rotate in opposite directions (cf. arrows in Fig. 2). However, as only O(2) anions move in the same direction (O(1) atoms do not rotate significantly)

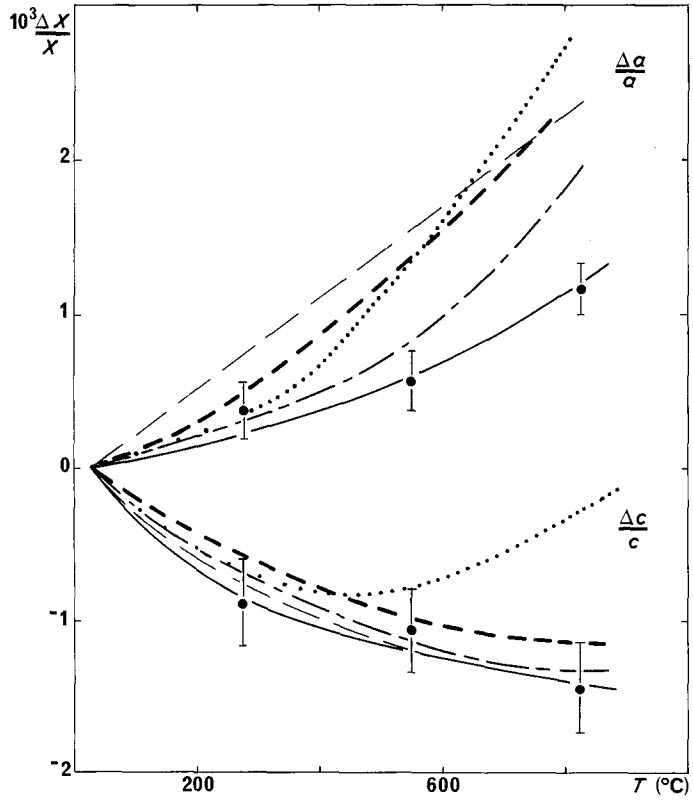

Figure 4 Thermal evolution of the lattice parameters for several pure or substituted cordierites: (. . .) [2], (– – –) [9], (— — —) [10], (— —) [11], (———) present work.

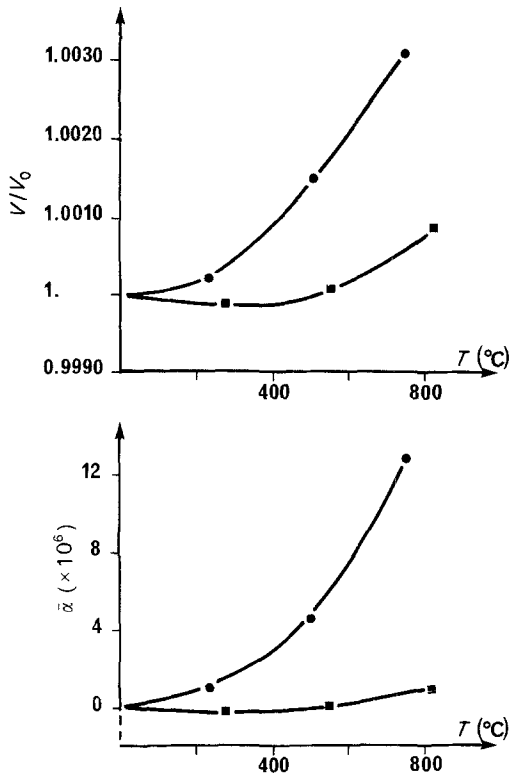

Figure 5 Thermal expansion of (■) our MK 25-substituted cordierite and (●) of pure hexagonal cordierite [9].

these displacements seem to correspond to a reorganization and a regularizaion of the $T(2)O_4$ tetrahedra (see σ values in Table III) within the six-membered rings, rather than to clockwise and counter-clockwise rotations of these rings in alternate layers. As we can see in Fig. 7 this regularization leads to an opposite evolution with increasing temperature of the heights H_M and $H_{T(2)}$ of the $T(1)O_4$–MgO_6 and $T(2)O_4$ rings respectively with the net result that there is a steady decrease in the c parameter.

A more detailed analysis of this thermal expansion may be done profitably by comparison with pure hexagonal cordierite [9] for which the phenomenon is fundamentally the same in nature. In both structures it results from a regular (pure cordierite) or nearly regular (MK25) expansion of the MgO_6 octahedra and a corresponding regularization of the $T(1)O_4$ tetrahedra. However, this expansion of the MgO_6 octahedra does not occur in the same way for the whole thermal domain. Two stages can be distinguished; the first stage and the second stage.

3.2.1. First stage: 20 to 300, 400° C

With increasing temperature, the MgO_6 octahedra expand anisotropically, i.e. mainly in the $x0y$ basal plane (expansion of horizontal $O(1)^2$–$O(1)^4$ edges and contraction of oblique $O(1)^1$–$O(1)^4$ and $O(1)^1$–$O(1)^2$ edges; see Fig. 8). This is allowed by the slight contraction and the regularization of the $T(1)O_4$ tetrahedra whose severe distortion and "abnormally high" volume at room temperature have been emphasized above. This evolution, which is achieved at the expense of a very short $O(1)^1$–$O(1)^2$ common edge, results in a flattening of the MgO_6–$T(1)O_4$ sheets (decrease of H_M in Fig. 7) and in a correlated thickening of $T(2)O_4$ sheets. This is mainly due to the vertical displacements of O(1) atoms, i.e. the increase of vertical O(1)–O(1) edges of these tetrahedra (see Table II). The extent of the evolution, however, is considerably more important for the MK25-substituted compound than for the pure cordierite. Two main reasons can be considered:

(i) the higher ionicity of bonds due to a higher aluminium rate in the $T(1)O_4$ and $T(2)O_4$ tetrahedra;

(ii) the presence of potassium atoms within the channels which prevents the inward movements of T(2) and O(2) atoms observed for pure cordierite (see Fig. 6) and therefore intensify the vertical movements of O(1) atoms.

3.2.2. Second stage: 300, 400 to 825° C

With increasing temperature, the MgO_6 octahedra can no longer expand anisotropically because of the strong electrostatic repulsions resulting from the very short $O(1)^1$–$O(1)^2$ shared edges which are generated.

In the case of pure cordierite they now expand isotropically, i.e. both oblique and horizontal edges increase simultaneously. As a consequence, an increase

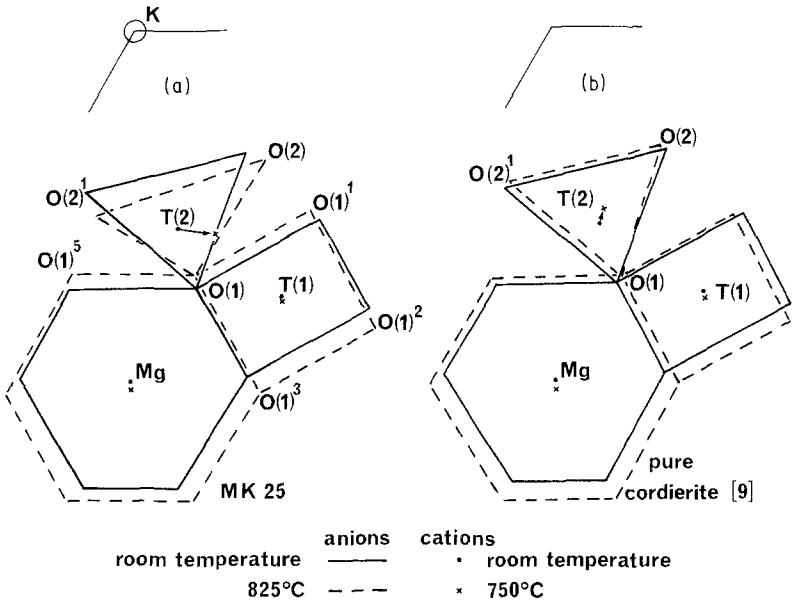

Figure 6 Projection onto the $x0y$ plane of the three basic polyhedra MgO_6, $T(1)O_4$ and $T(2)O_4$, (a) at room temperature and 825° C for the MK25 cordierite and (b) at room temperature and 750° C for pure cordierite [9]. Displacements of the 825 and 750° C atom positions from the room temperature positions have been magnified 20 times.

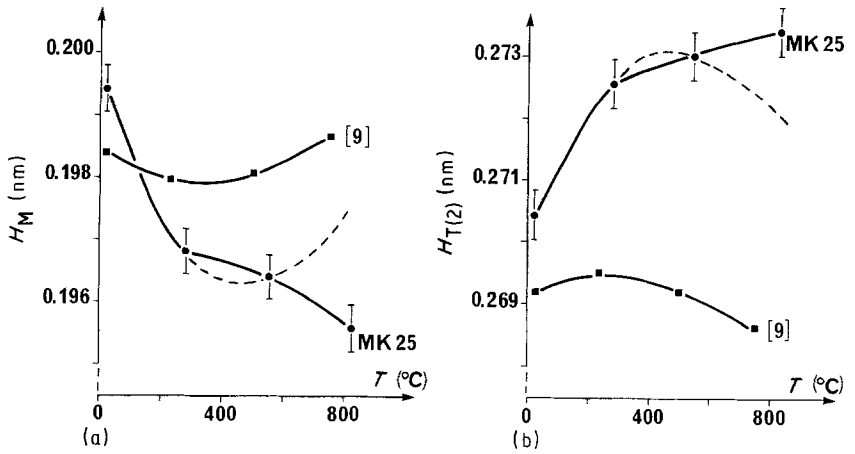

Figure 7 Thermal evolution of the heights (a) H_M and (b) $H_{T(2)}$ of, respectively, the "$T(1)O_4$ + MgO_6" and $T(2)O_4$ sheets in MK25 and pure cordierite [9].

of $H_M = H_{T(1)}$ and a decrease of $H_{T(2)}$ are therefore observed.

In the case of substituted MK25 cordierite, the same change occurs probably at about 400° C. But it cannot continue at higher temperatures because of the onset of a new phenomenon, apparently not observed for pure cordierite, i.e. the partial Al/Si ordering within the $T(1)O_4$ and $T(2)O_4$ tetrahedra. The $T(2)O_4$ tetrahedra are enriched with silicon atoms to the detriment of $T(1)O_4$ tetrahedra (see occupancies in Table I), so that

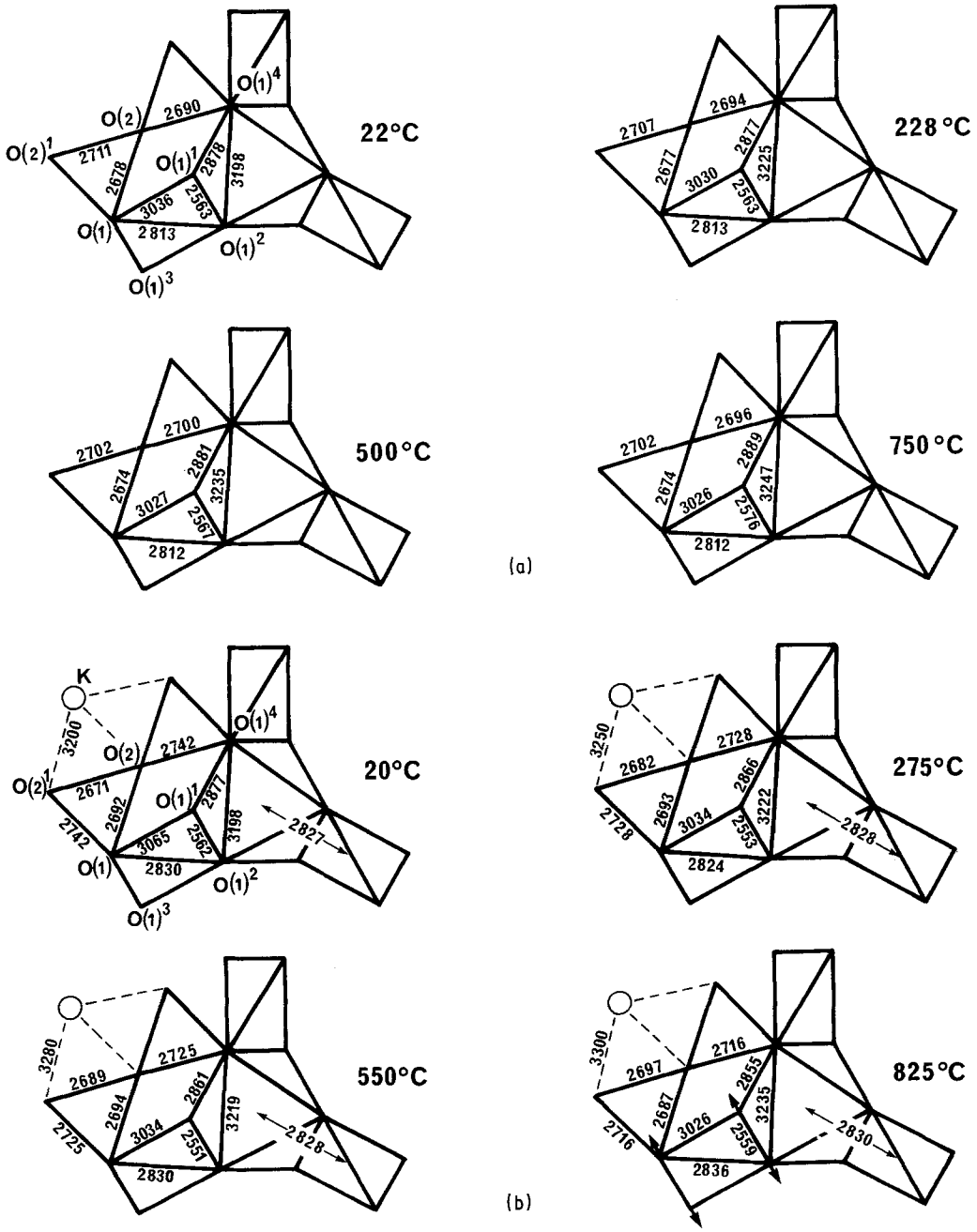

Figure 8 Changes with increasing temperature in the various polyhedra of (a) pure hexagonal cordierite [9], (b) substituted MK 25 cordierite (bond lengths are given in 10^4 nm).

the mean T(2)–O distance decreases whereas the mean T(1)–O distance increases. It results in an inward movement of O(1) atoms (see arrows in Fig. 8b, 825° C) allowing, at the same time, the MgO_6 and $T(1)O_4$ polyhedra to flatten again and the too short $O(1)^1$–$O(1)^2$ shared edges to increase, leading to a new regularization of the $T(1)O_4$ and $T(2)O_4$ tetrahedra. As we can see in Fig. 7, the thermal evolution of the heights H_M and $H_{T(2)}$ of the two sheets its therefore opposite to that observed in pure cordierite. However, it is highly probable that without this ordering it would have been in perfect agreement with the hypothetical curves shown as dashed lines.

4. Conclusion

The thermal evolution of MK25-substituted cordierite is essentially of the same nature as for pure hexagonal cordierite. It expresses the response, via their regularization, of the $T(1)O_4$ and $T(2)O_4$ tetrahedra, to the expansion of MgO_6 octahedra. For both compounds this response seems to be optimum at about 300 to 400° C. Nevertheless, the insertion of potassium atoms within the channels plays a very important role in the thermal behaviour of MK25 cordierite.

Directly, by preventing the inward movements of T(2) and O(2) atoms, indirectly by increasing the ionic character of (Al, Si)–O bonds, it accentuates the reorganization of polyhedra and then allows a better compensation of the a parameter increase by the c parameter decrease. The net result is a very low mean thermal expansion coefficent (the lowest ever observed for cordierite-type materials: $\bar{\alpha} = 0.4$ p.p.m. from 20 up to 825° C).

However, the thermal behaviour of this type of phase, and therefore the thermal expansion coefficient values are strongly dependent on the Al/Si ordering degree and hence on the thermal history of the samples [22, 23]. A systematic study of this order by transmission electron microscopy, infrared and Raman spectroscopy and by high-resolution nuclear magnetic resonance (magic angle spinning) is in progress.

References

1. R. MORREL, *Proc. Br. Ceram. Soc.* **28** (1979) 53.
2. D. L. EVANS, G. R. FISHER, J. E. GEIGER and F. W. MARTIN, *J. Amer. Ceram. Soc.* **63** (1980) 629.
3. B. H. MUSSLER and M. W. SHAFER, *Amer. Ceram. Soc. Bull.* **63** (1984) 705.
4. G. V. GIBBS, *Amer. Mineral.* **51** (1966) 1069.
5. E. P. MAEGHER and G. V. GIBBS, *Can. Mineral.* **15** (1977) 43.
6. J. P. COHEN, F. K. ROSS and G. V. GIBBS, *Amer. Mineral.* **62** (1977) 67.
7. M. F. HOCHELLA Jr, G. G. BROWN Jr, F. K. ROSS and G. V. GIBBS, *ibid.* **64** (1979) 337.
8. J. H. WALLACE and H. R. WENK, *ibid.* **65** (1980) 96.
9. P. PREDECKI, J. HAAS, J. FABER Jr and R. L. HITTERMAN, *J. Amer. Ceram. Soc.* **70** (1987) 175.
10. M. E. MILBERG and H. D. BLAIR, *ibid.* **60** (1977) 372.
11. J. D. LEE and J. L. PENTECOST, *ibid.* **59** (1976) 183.
12. H. IKAWA, T. OTAGIRI, O. IMAI, M. SUZUKI, K. URABE and S. UDAGAWA, *J. Amer. Ceram. Soc.* **69** (1986) 492.
13. P. PREDECKI, J. HAAS, J. FABER Jr and R. L. HITTERMAN, *Adv. X-ray Anal.* **29** (1986) 173.
14. Y. H. KIM, D. MERCURIO, J. P. MERCURIO and B. FRIT, *Mater. Res. Bull.* **19** (1984) 209.
15. Y. H. KIM, J. P. MERCURIO and C. GAULT, *Ceram. Int.* **11** (1985) 27.
16. J. P. MERCURIO, D. MERCURIO, B. FRIT, Y. H. KIM and G. ROULT, High Tech Ceramics, Material Science Monographs, 38 (Elsevier Science, Amsterdam, 1987) p. 361.
17. J. HAAS, P. PREDECKI, J. FABER JR and R. L. HITTERMAN, *Adv. X-ray Anal.* **29** (1986) 395.
18. G. ROULT and J. L. BUEVOZ, *Rev. Phys. Appl.* **12** (1977) 581.
19. H. M. RIETVELD, *J. Appl. Crystallogr.* **2** (1969) 65.
20. R. M. HAZEN and L. W. FINGER, "Comparative Crystal Chemistry" (Wiley, New York, 1982) p. 86.
21. K. ROBINSON, G. V. GIBBS and P. H. RIBBE, *Science* **172** (1971) 567.
22. C. A. FYFE, G. C. GOBBI and A. PUTNIS, *J. Amer. Chem. Soc.* **108** (1986) 3218.
23. A. PUTNIS, E. SALJE, S. A. T. REDFERN, C. A. FYFE and H. STROBL, *Phys. Chem. Minerals* **14** (1987) 446.

Received 2 August 1988
and accepted 5 January 1989